JOURNAL OF AIRCRAFT
Vol. 37, No. 2, March–April 2000

Nonlinear Rate and Amplitude Effects on a Generic Combat Aircraft Model

Lars E. Ericsson*
Mountain View, California 94040
and
Martin E. Beyers†
Institute for Aerospace Research, Ottawa, Ontario K1A 0R6, Canada

A study has been made of the unusual results obtained in large-amplitude oscillatory coning and pitching tests of a generic combat aircraft model. The analysis shows that the observed highly nonlinear effects of angular amplitude and rate on the unsteady aerodynamics can be explained by using the knowledge of unsteady separated flow physics gained from one-degree-of-freedom dynamic experiments. Anomalous effects are produced by the wind-tunnel testing practice of using boundary-layer trips, which introduces a unique sensitivity to boundary-layer transition not found in full-scale flight.

Nomenclature

b = wing span
c = reference length, mean aerodynamic chord
c_0 = wing root chord
d = maximum body diameter
$d(x)$ = local body diameter
l = rolling moment, coefficient $C_l = l/(\rho_\infty U_\infty^2/2)Sb$
m = pitching moment, coefficient $C_m = m/(\rho_\infty U_\infty^2/2)Sc$
N = normal force, coefficient $C_N = N/(\rho_\infty U_\infty^2/2)S$
n = yawing moment, coefficient $C_n = n/(\rho_\infty U_\infty^2/2)Sb$
p = static pressure, coefficient $C_p = (p - p_0)/(\rho_\infty U_\infty^2/2)$
Re = Reynolds number based on d and freestream conditions; $Re(x)$ based on local diameter $d(x)$ (Fig. 11)
S = reference area, projected wing area, $\pi d^2/4$ for body alone
t = time
U = velocity
V = crossflow velocity
x = axial body-fixed coordinate
Y = side force: coefficient $C_Y = Y/(\rho_\infty U_\infty^2/2)S$; $c_y = \partial C_Y/\partial\xi$
$z(x)$ = cross-sectional height above flow stagnation point
α = angle of attack
$\dot{\alpha}$ = $\partial\alpha/\partial t$
β = angle of sideslip
Γ = vortex circulation (Fig. 7)
Δ = increment
ζ = dimensionless z coordinate, $z/d(x)$ (Fig. 11)
ξ = dimensionless x coordinate, x/c_0
ρ = air density
φ = azimuth
ψ = coning angle
Ω = dimensionless coning rate, $\omega b/2U_\infty$
ω = coning rate, $\partial\psi/\partial t$

Subscripts

I = initial
LS = laminar separation
TR = transition
TS = turbulent separation
t = trip
VB = vortex breakdown
∞ = freestream conditions

Received 1 May 1998; revision received 5 April 1999; accepted for publication 30 August 1999.

*Engineering Consultant. Fellow AIAA.
†Head, Aircraft Aerodynamics, Aerodynamics Laboratory. Senior Member AIAA.

Introduction

In recently completed dynamic wind-tunnel tests[1] to explore the highly nonlinear unsteady aerodynamics prevailing on a generic combat aircraft model (Fig. 1) at high angles of attack, the oscillatory-coning test technique[2] was used to generate sinusoidal variations of angle of attack and sideslip superimposed upon the regular coning motion. In another test rig the model was driven in large amplitude pitch oscillations. The tests demonstrated that at high angles of attack the highly nonlinear effects of amplitude and angular rate are very complex. Although the oscillatory coning results are not fully representative of high-alpha maneuvers, the methodology used here to interpret the unsteady aerodynamics of complex motions is directly applicable.

Discussion

The aerodynamics of the combat aircraft model[1] become highly nonlinear at $\alpha > 19$ deg because of the effects of separated flow and vortex bursting. The use of boundary-layer trips and nose strakes (Fig. 1) further complicated the experimental unsteady aerodynamics.[3] Significant time-history effects added to the complexity, making the rotary aerodynamics very difficult to interpret. In what follows unsteady flow concepts are presented that can explain the unusual aerodynamic characteristics measured in rotary tests.[1]

Effect of Sideslip

The nonlinear static aerodynamics at 10 deg $< \alpha <$ 40 deg and $\beta = \pm 10$ deg (Fig. 2) can be explained by the sideslip effects discussed in Ref. 4. Flow visualization results[1] for symmetric conditions ($\beta = 0$) show vortex breakdown to start at the trailing edge at $\alpha = 19$ deg and move to the LEX-wing junction at $\alpha = 39$ deg, initiating the stall of the complete wing (Fig. 3). Drawing from earlier experience with double-delta wings,[4] one can construct the conceptual flow physics illustrated in Fig. 4. At $\alpha < 15$ deg no breakdown occurs on the wing, and the regular sideslip effect[5,6] generates a positive rolling moment at $\beta = -10$ deg. At this angle of sideslip, vortex breakdown occurs early on the windward side and will be extensive at $\alpha > 20$ deg (Fig. 4). The windward wing half will be completely stalled at $\alpha \approx 30$ deg, long before the zero-sideslip value $\alpha = 39$ deg

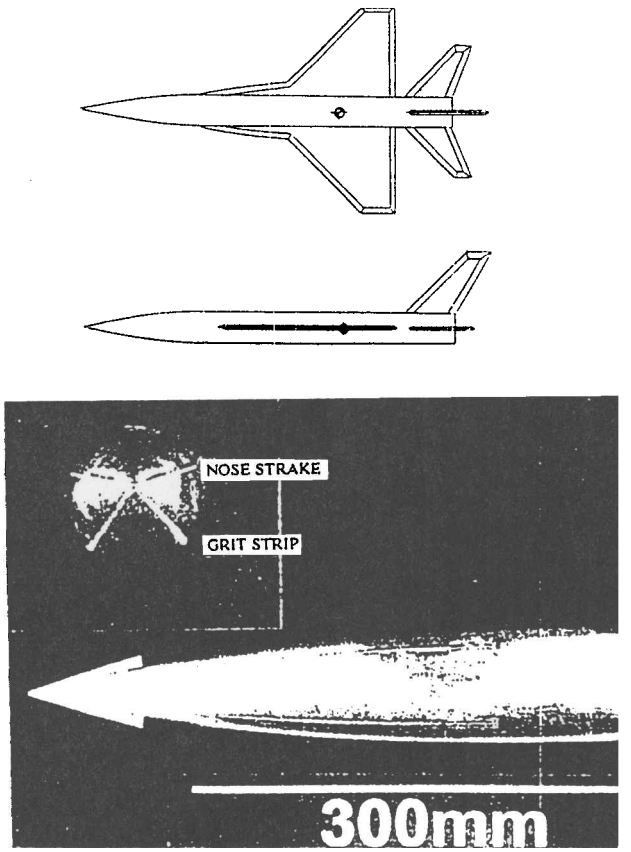

Fig. 1 Generic combat aircraft model with nose strakes and grit strips at $\phi_l = \pm 40$ deg (Ref. 1).

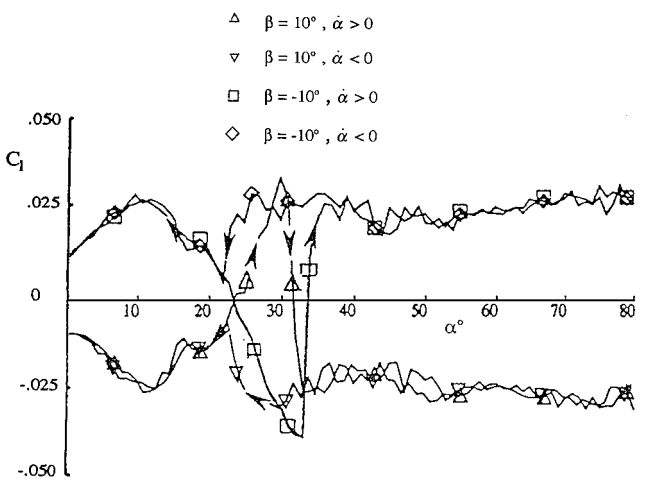

Fig. 2 Effect of sideslip and pitch rate on $C_l(\alpha)$ (Ref. 1).

(Fig. 3). At $\alpha \approx 30$ deg the leeward wing half has just started to experience vortex breakdown. The stalled windward and unstalled leeward wing halves together produce the minimum C_l value in Fig. 4. That the leeside wing half becomes completely stalled at or before the value for $\beta = 0$ ($\alpha = 39$ deg) is probably a result of the body-shadow effect. Going back to Fig. 2, one still needs to find a reason for the large α hysteresis in the experimental results.

When the angle of attack is increased to $\alpha \geq 35$ deg, the vortex breakdown moves to the apex also on the leeside wing half. As a result, the lift that was generated by the vortex on that wing half, upstream and downstream of a spiral vortex breakdown, is wiped out,[7] as in the example in Fig. 5d, completely eliminating the associated contribution to the negative rolling moment. The α hysteresis in Figs. 2 and 4 is of the usual type, showing the reestablishment

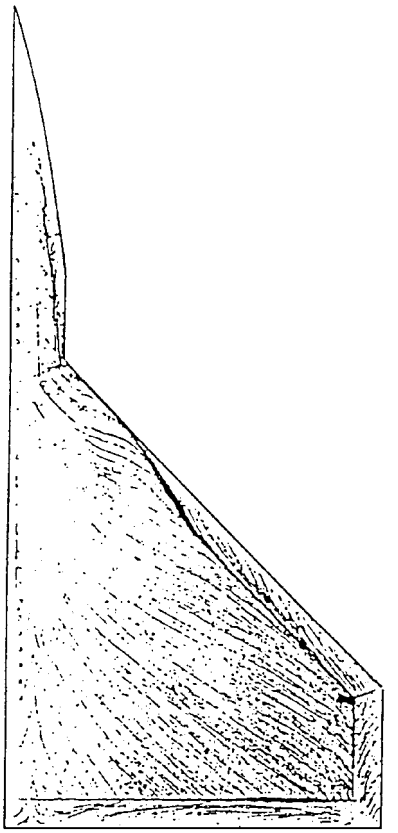

Fig. 3 Flow patterns at α = 39 deg (Ref. 1).

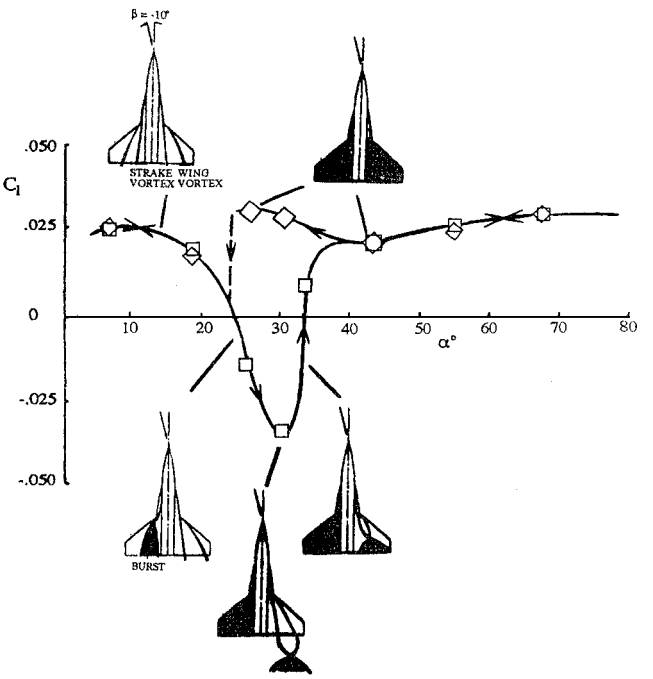

Fig. 4 Conceptual vortex characteristics for the measured $C_l(\alpha)$ at $\beta = -10$ deg.

of unburst vortices to take place at an angle of attack far below that for starting vortex breakdown. Once three-dimensional stall has been established at $\alpha \geq 35$ deg, the spiral type of vortex breakdown, shown in Figs. 5a–5c, cannot be reestablished on the downstroke.

The C_l characteristics in Figs. 2 and 4 indicate that both wing halves stay completely stalled until the angle of attack has been decreased below $\alpha = 25$ deg, toward the value $\alpha = 19$ deg, where vortex breakdown ceases to occur on the wing at $\beta = 0$.

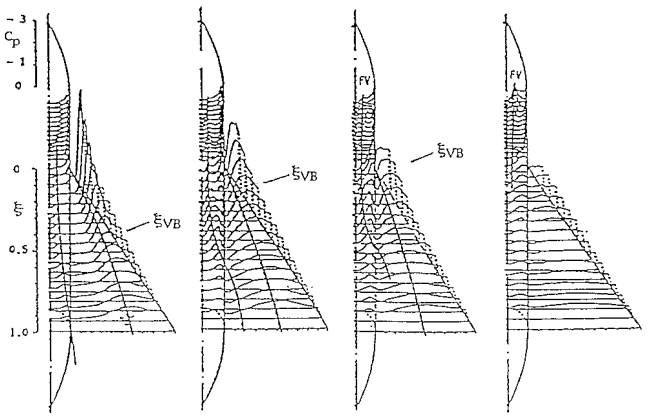

a) α = 19.3 deg b) α = 29.1 deg c) α = 34.1 deg d) α = 39.1 deg

Fig. 5 Three-dimensional stall of a delta-wing-body configuration[7] (VB = vortex breakdown).

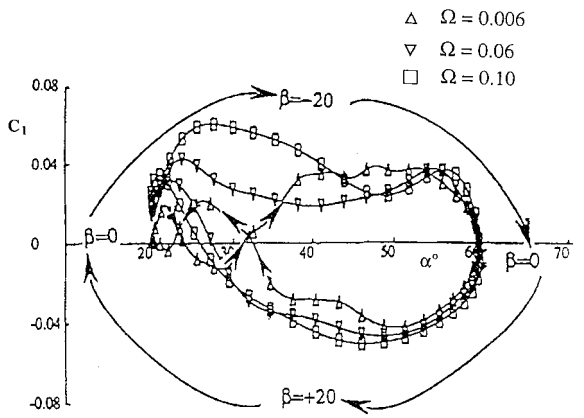

Fig. 6 Effect of oscillatory coning rate on $C_l(\alpha)$ (Ref. 1).

Effect of Coning Rate

The oscillatory coning results[1] show that the sign change of the $C_l(\beta)$ characteristics observed at 25 deg $< \alpha <$ 35 deg for $\Omega = 0$ (Fig. 2) also occurred for $\Omega = 0.006$ (Fig. 6), but does not occur when the rotation rate is increased to and beyond $\Omega = 0.06$. The likely reason for this is that the coning-induced sideslip changes the effective leading-edge geometry (The direction of the β variation -20 deg $\leq \beta \leq 20$ deg is indicated in Fig. 6). The rate-induced effects will be largest close to the upper and lower ends of the tested α range, where $|\beta|$ is largest. Because of convective time-lag effects, conceptually similar to those for a rolling 65-deg delta wing,[8,9] the rate-induced effect will be felt over the wing progressively later in the motion cycle as the rate is increased. This could explain the dramatic Ω effect on the rolling moment at $\alpha > 20$ deg, which completely eliminates the static nonlinear $C_l(\alpha)$ loops existing for $\Omega = 0.006$. In the range 20 deg $< \alpha <$ 40 deg, where $\dot{\beta} < 0$ during the upstroke ($\dot{\alpha} > 0$ in Fig. 6), the negative yaw rate will deform the Dynamically Equivalent Steady (DES)[10] planform to take the shape shown in Fig. 7, generating a Gothic wing geometry on the windward side and an ogee type on the leeward side, with the leading-edge vortices on the sideslipping wing effectively oriented as depicted in Fig. 7. Thus, in the absence of vortex breakdown, the negative yaw rate at 20 deg $< \alpha <$ 40 deg for $\dot{\alpha} > 0$ will for $\Omega \geq 0.06$ generate an increment $\Delta C_l > 0$ relative to the near-steady rolling moment at $\Omega = 0.006$, eliminating the branch $C_l(\alpha) < 0$. (It can be shown that vortex breakdown will be delayed on the Gothic wing half and promoted on the ogee-shaped side, further contributing to the positive C_l increment.) The corresponding effect on the backstroke $\dot{\alpha} < 0$ eliminates the branch $C_l(\alpha) > 0$. This explains the absence of the extra $C_l(\alpha)$ loops observed for $\Omega = 0.006$. The experimental results in Fig. 6 also show the expected increased magnitude of the rate-induced ΔC_l with increasing Ω. At high alpha (33 deg $< \alpha <$ 55 deg)

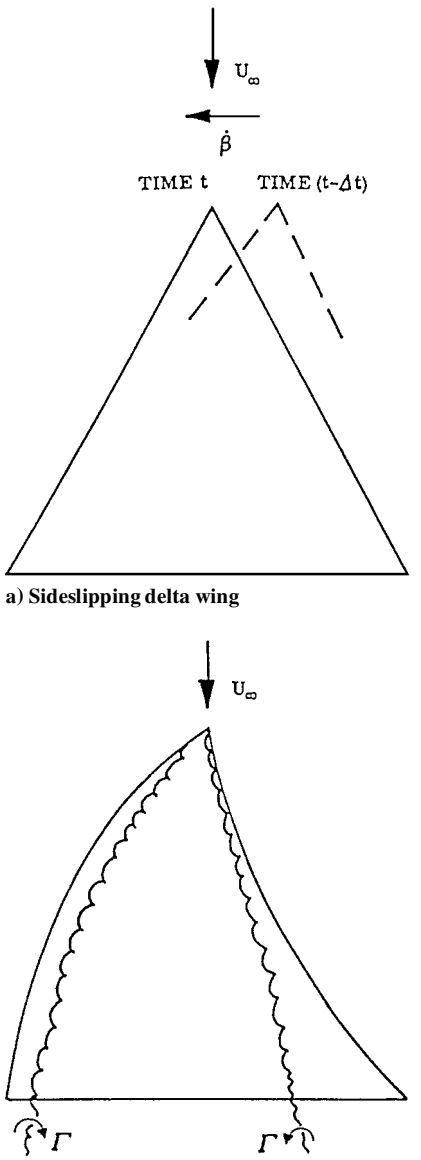

a) Sideslipping delta wing

b) Dynamically equivalent steady wing

Fig. 7 Dynamically equivalent steady leading-edge geometry of yawing delta wing.

the generation of lift on the wing through the effect of sideslip on the upwash produced by the leading edge extension (LEX) is coupled to the interaction between the attached forebody vortex and the LEX vortex.[3] This coupling is evident in the correspondence between C_l and C_n loops at high alpha.[1] The experimental results in Figs. 3 and 6 indicate that a maneuvering combat aircraft is likely to experience significant motion-induced coupling effects[11] at moderately high angles of attack.

Slender Forebody Aerodynamics

The complicated nature of the loads induced on a slender forebody in pitch oscillations are well illustrated by the C_n results in Fig. 8, obtained on the model with nose strakes and grit strips[1] (Fig. 1). The data are unusual in two respects. First, a nonzero static yawing moment is measured at $\beta = 0$ for $\alpha >$ 45 deg, even though the strakes force the flow separation to be symmetric at the nose tip.[12] The nose strakes only delay the occurrence of the separation asymmetry from $\alpha >$ 30 deg, expected for the 28.5 deg complete apex angle,[13] to $\alpha \geq$45 deg (slow alpha sweep in Fig. 8). This is consistent with experimental results for the X-31 aircraft,[14] indicating that a limited range exists at high alpha in which steady asymmetric crossflow separation can develop aft of the nose region

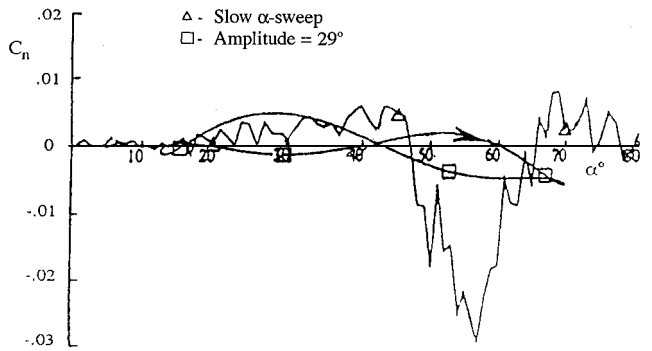

Fig. 8 Effect of large-amplitude oscillations in pitch on $C_n(\alpha)$ (Ref. 1).

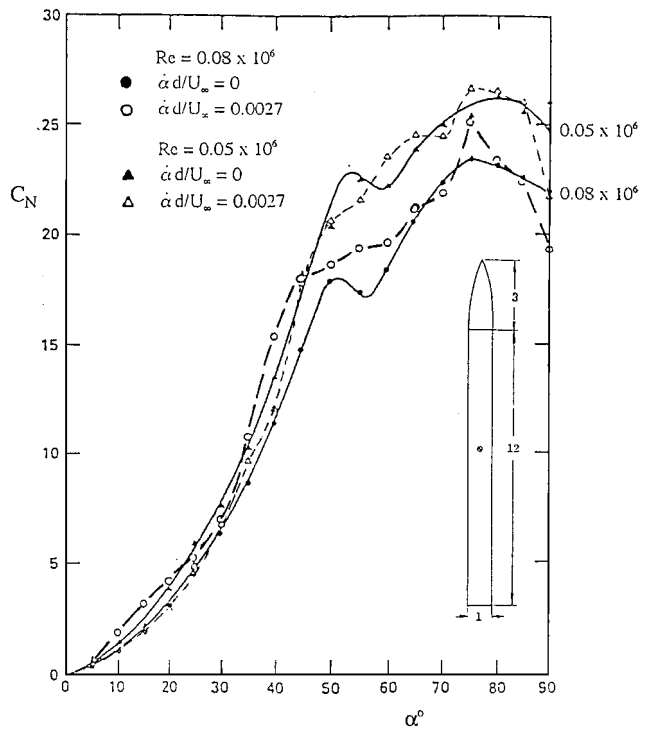

Fig. 9 Pitch-rate effect on the normal force of an ogive cylinder at critical flow conditions.[15]

affected by the strakes. Flow visualization results at $\alpha = 46$ deg for the aircraft model with a clean forebody[12] show that a new vortex pair is being generated two calibers downstream of the nose tip. This is in basic agreement with existing experimental evidence.[13] If the forebody is long enough, the presence of the symmetric first vortex pair, produced by the nose strakes, can only delay, not prevent, the occurrence of asymmetric flow separation farther downstream. The location where the second vortex pair starts on the clean forebody in the present case is approximately one strake length behind the trailing edges of the nose strakes.[12] It is more challenging to explain the other result in Fig. 8, i.e., the capability of a very modest pitch rate to eliminate the asymmetric crossflow separation existing at 45 deg $< \alpha <$ 65 deg for essentially static flow conditions (slow alpha sweep). As the $C_n(\alpha)$ loops above and below $\alpha = 40$ deg are quite similar, there cannot be any significant effect of forebody flow asymmetry at $\alpha > 40$ deg.

Experimental results for an ogive cylinder[15,16] (Fig. 9) show that the modest pitch-up rate $\dot{\alpha}d/U_\infty = 0.0027$ significantly changed the crossflow separation characteristics from those existing at $\dot{\alpha} = 0$. Apparently, the crossflow acceleration, generated by the pitch-up motion, had an effect similar to that of nose strakes[17] (Fig. 10), preventing the asymmetric flow separation with associated side force and increased normal force from developing. The crossflow separation process can be simulated using the impulsively started cylinder

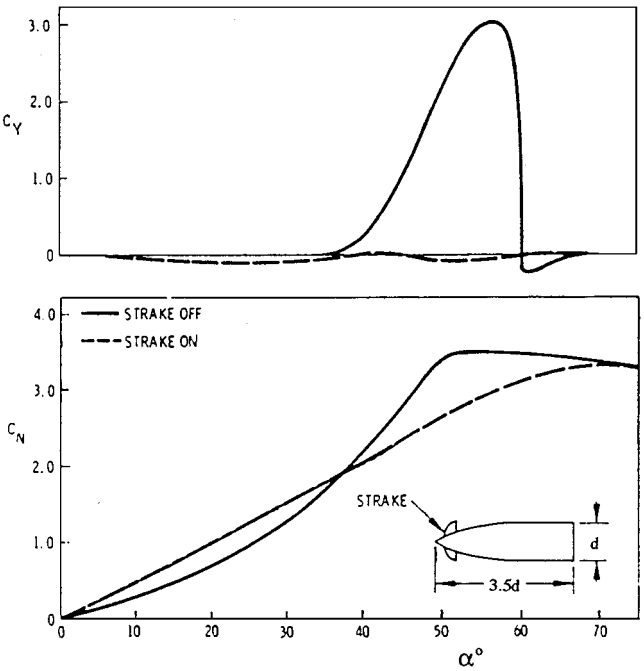

Fig. 10 Effect of nose strakes on normal and side force coefficients for a pointed 3.5-caliber tangent ogive.[17]

flow analogy.[18,19] In that case the crossflow velocity V is a function of the initial velocity $V_I = U_\infty \sin \alpha$, and the crossflow acceleration can be written as

$$V = f(V_I) \tag{1a}$$

$$\frac{dV}{dt} = \frac{\partial f}{\partial V_I} U_\infty \dot{\alpha} \cos \alpha \tag{1b}$$

Equation (1b) shows that the crossflow acceleration is largest at $\alpha = 0$ and becomes zero at $\alpha = 90$ deg. This is in agreement with the data trend in Fig. 9, where the largest difference from the static normal force occurs at low angles of attack, and becomes neglible at $\alpha \geq 60$ deg, where the increased data scatter is the likely result of Karman-type flow instability.[13] The kink at $\alpha > 50$ deg in the static $C_N(\alpha)$ curves is the result of the liftoff of one asymmetric vortex, allowing the other, lower vortex to move inboard, thereby generating more normal force. This data trend is clearly exhibited by the experimental results[17] in Fig. 10. The cylindrical afterbody produced the additional C_N increase at higher angles of attack in Fig. 9.

One question that needs to be answered is why the accelerated flow effect is so much larger at $Re = 0.08 \times 10^6$ than at $Re = 0.05 \times 10^6$. The quoted[15] 6% decrease of the freestream speed when the model was pitched from $\alpha = 0$ to 90 deg indicates that the model blockage was substantial, suggesting that the associated increased turbulence level could have been responsible for the early establishment of critical crossflow conditions. With that scenario the experimental results in Fig. 9 suggest that at $Re = 0.08 \times 10^6$ the static characteristics were obtained at critical flow conditions, whereas at $Re = 0.05 \times 10^6$ laminar flow conditions prevailed. This is consistent with the fact that the crossflow drag at $\alpha = 90$ deg resulted in 10% lower C_N at $Re = 0.08 \times 10^6$ than at $Re = 0.05 \times 10^6$. Furthermore, at $Re = 0.08 \times 10^6$ it appears that the accelerated flow effects during pitch up were powerful enough to produce laminar flow conditions, generating C_N values equal to or larger than the static values for $Re = 0.05 \times 10^6$ at $\alpha < 50$ deg. That the crossflow conditions on the clean forebody of the combat aircraft model (Fig. 1) were close to the critical range at $Re = 0.2 \times 10^6$ can be verified by a comparison with the force data at $Re = 0.15$ and 0.30×10^6 (Ref. 12). The presence of the trips at $\varphi_t = \pm 40$ deg on the forebody (Fig. 1) could have played a significant role in establishing critical crossflow conditions at $Re = 0.2 \times 10^6$.

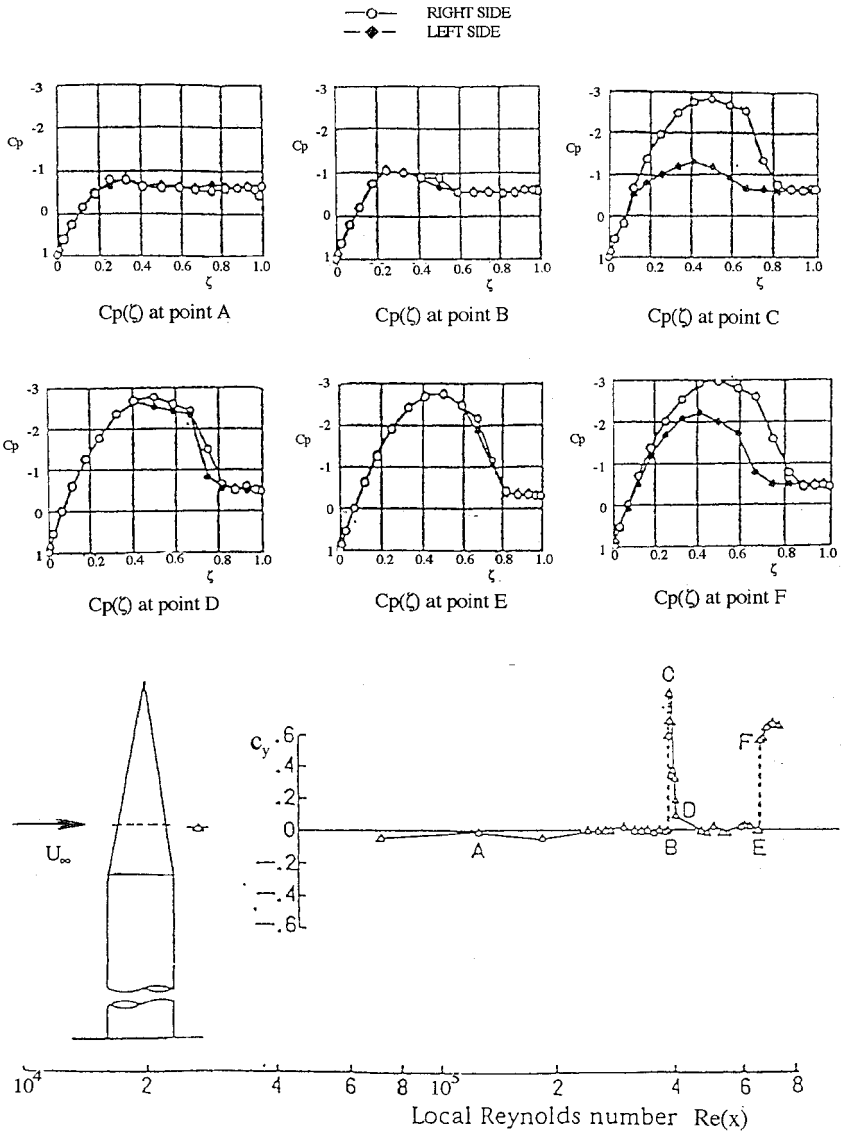

Fig. 11 Cross-sectional pressure distribution on a 5.4-deg cone cylinder at α = 90 deg (Ref. 20).

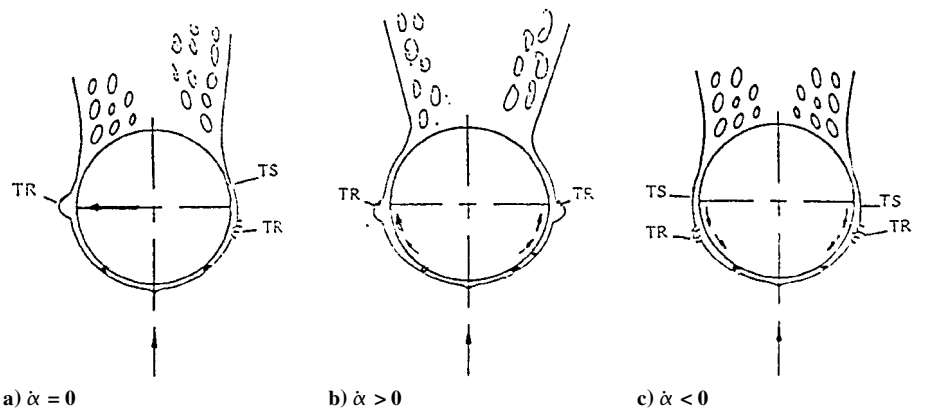

a) $\dot{\alpha} = 0$ b) $\dot{\alpha} > 0$ c) $\dot{\alpha} < 0$

Fig. 12 Conceptual pitch-rate-induced effects on the crossflow separation at α > 46 deg on the combat aircraft model with nose strakes and with grit strips at ϕ_t = ± 40 deg (TS = turbulent separation, TR = transition).

By analogy with the experimental results[20] in Fig. 11, one can for $\alpha > 45$ deg in Fig. 8 construct the conceptual crossflow geometries shown in Fig. 12. At $\dot{\alpha} = 0$ the crossflow geometry giving a pressure distribution corresponding to point F in Fig. 11 is established. This supercritical/critical separation geometry (Fig. 12a) generates a large side force (although not as large as that at point C, generated by the subcritical/critical separation asymmetry). This produces a yawing moment of large magnitude (slow α sweep in Fig. 8). Because the boundary layer downstream of the trips is at the point of transition, the accelerated flow effect is likely to be large. Figure 11 (point F) shows that it takes a minuscule decrease of the crossflow Reynolds number to go back to the critical/critical (point E) symmetric crossflow separation geometry. Likewise, a small Reynolds-number increase would produce the symmetric supercritical/supercritical crossflow separation geometry. Consequently, a very modest accelerated flow effect could have been able to cause a

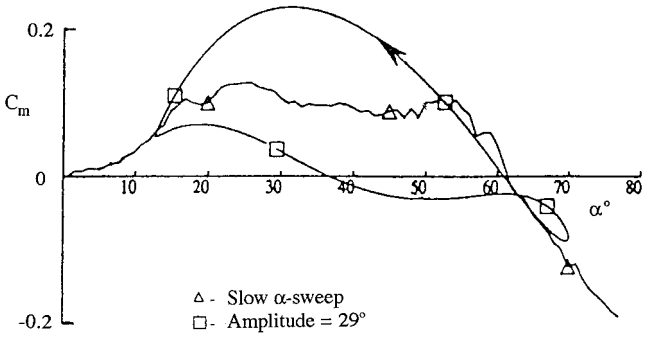

Fig. 13 Effect of large amplitude pitch oscillations on $C_m(\alpha)$ (Ref. 1).

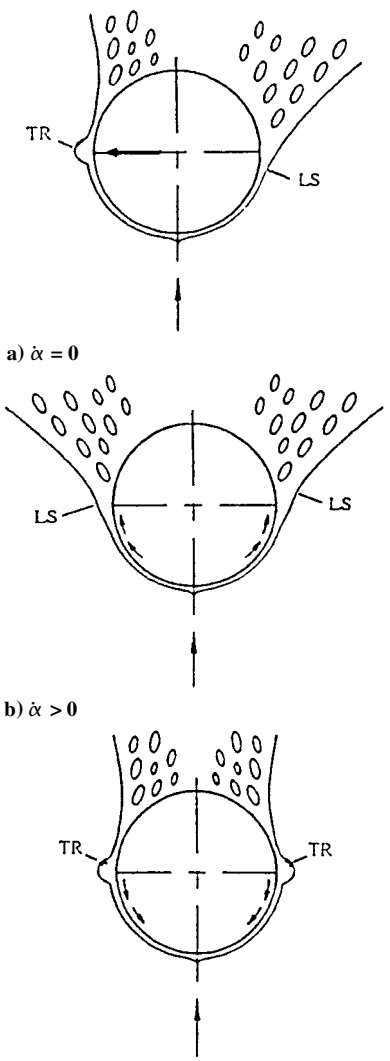

Fig. 14 Conceptual pitch-rate-induced effects on the crossflow separation at $\alpha > 46$ deg on the combat aircraft model with nose strakes but without grit strips (LS = laminar separation, TR = transition).

complete change of flow separation geometry. In the pitch-up case $\dot{\alpha} > 0$ (Fig. 12b), the favorable accelerated flow effect will delay transition, permitting the critical flow separation to be established on both sides to produce the minimum normal force. In contrast, during the pitch-down $\dot{\alpha} < 0$ (Fig. 12c), the adverse decelerated flow effect will promote transition, establishing the supercritical/supercritical separation geometry shown in Fig. 12c, which generates a normal force that is larger than in the static case and significantly larger than that for $\dot{\alpha} > 0$ (Fig. 12b). As a result, the local normal force generated by the forebody would be decreased below the static value during the upstroke $\dot{\alpha} > 0$ and increased above it during the downstroke, all in agreement with the experimental $C_m(\alpha)$ in Fig. 13; the dominant effect on C_m, for the moment reference axis of the present model (Fig. 1), is the change of the local normal force on the slender forebody.

According to the preceding discussion, the grit strips at $\varphi_t = \pm 40$ deg contributed to the experimental data trends in Figs. 6 and 13. One naturally asks oneself what the experimental results in Figs. 6 and 13 would have looked like in the absence of these grit strips. For the clean forebody the crossflow conditions are known to be subcritical[1,12] at the test Reynolds number $Re = 0.2 \times 10^6$, with the separated-flow topology shown in Fig. 14b, corresponding to a point between A and B in Fig. 11. In that case the accelerated flow effect would be ineffective, and the $C_m(\alpha)$ results would be similar for $\dot{\alpha} = 0$ and $\dot{\alpha} \neq 0$. Note, however, that if the test had been performed at a slightly higher Reynolds number, corresponding to point C in Fig. 11, the crossflow separation topology sketched in Fig. 14a would have resulted. In that case the minute pitch-rate-induced accelerated/decelerated flow effects could have been sufficient to cause a change of separation geometry (from point C in Fig. 11 to points B or D). This would imply that during the upstroke ($\dot{\alpha} > 0$) the favorable accelerated flow effect could have delayed transition, changing the asymmetric critical/subcritical separation in Fig. 14a back to the subcritical/subcritical flow separation sketched in Fig. 14b, which would have generated the maximum local normal force. During the downstroke ($\dot{\alpha} < 0$), on the other hand, the adverse decelerated flow effect would promote transition, possibly changing the subcritical/critical separation at $\dot{\alpha} = 0$ to a critical/critical crossflow geometry (Fig. 14c), generating the minimum local normal force. Thus, the local normal force generated by the forebody would be increased above the static value during the upstroke $\dot{\alpha} > 0$ and reduced below it during the downstroke $\dot{\alpha} < 0$, all contrary to the experimental C_m results in Fig. 14. Of course, at full-scale Reynolds numbers neither one of these scenarios could be realized, adding another example to the scaling problems discussed in Ref. 3 for the generic combat aircraft model[1] (Fig. 1) and in Ref. 21 for subscale tests in general. The test engineer should be warned to avoid flow conditions in subscale tests that introduce boundary-layer transition effects not present in full-scale flight.

Conclusions

A study of the dynamic test results obtained for a subscale combat aircraft model shows that the highly nonlinear effect on the unsteady aerodynamics of angular rate and oscillation amplitude can be explained by applying the knowledge gained from existing results for one-degree-of-freedom dynamic tests with subscale models of missile and wing geometries. Although the test results analyzed are not at all representative of full-scale flight conditions, largely because of the conventional use of boundary-layer trips, the methodology used is fully applicable to the more straightforward analysis of the unsteady aerodynamics at full-scale Reynolds numbers.

References

[1] "Cooperative Programme on Dynamic Wind Tunnel Experiments for Maneuvering Aircraft," AGARD-AR-305, Oct. 1996.

[2] Tristrant, D., and Beyers, M. E., "Oscillatory Coning," AGARD-AR-265, Dec. 1990, Chap. 4, pp. 69–76.

[3] Ericsson, L. E., and Beyers, M. E., "Wind Tunnel Aerodynamics in Rotary Tests of Combat Aircraft Models," *Journal of Aircraft*, Vol. 35, No. 4, 1998, pp. 521–528.

[4] Ericsson, L. E., "Vortex Characteristics of Pitching Double-Delta Wings," *Journal of Aircraft*, Vol. 36, No. 2, 1999, pp. 349–356.

[5] Ericsson, L. E., and Reding, J. P., "Approximate Nonlinear Slender Wing Aerodynamics," *Journal of Aircraft*, Vol. 14, No. 12, 1977, pp. 1197–1204.

[6] Ericsson, L. E., and King, H. H. C., "Rapid Prediction of High-Alpha Unsteady Aerodynamics of Slender-Wing Aircraft," *Journal of Aircraft*, Vol. 29, No. 11, 1992, pp. 85–92.

[7] Bergmann, B., Hummel, D., and Oelker, H.-Chr., "Vortex Formation over a Close-Coupled Canard-Wing-Body Configuration in Unsymmetrical Flow," AGARD-CP-494, Paper 14, July 1991.

[8] Ericsson, L. E., "Flow Physics of Critical States for Rolling Delta Wings," *Journal of Aircraft*, Vol. 32, No. 3, 1995, pp. 603–610.

[9] Ericsson, L. E., "Time History Effects on a 65 Deg Delta-Wing-Body Configuration," *Journal of Aircraft*, Vol. 36, No. 3, 1999, pp. 489–495.

[10]Ericsson, L. E., "Vortex Breakdown Dynamics on Pitching Delta Wings," AIAA Paper 95-1777, June 1995.

[11]Ericsson, L. E., and Beyers, M. E., "Conceptual Fluid/Motion Coupling in the Herbst Supermaneuver," *Journal of Aircraft*, Vol. 34, No. 3, 1997, pp. 271–277.

[12]Cai, H. J., and Beyers, M. E., "Oscillatory Experiments on the AGARD WG16 CA Model," National Research Council Canada, IAR-AN-83, Sept. 1995.

[13]Ericsson, L. E., and Reding, J. P., "Asymmetric Flow Separation and Vortex Shedding on Bodies of Revolution," *Tactical Missile Aerodynamics: General Topics*, edited by M. J. Hemsch, Vol. 141, Progress in Astronautics and Aeronautics, 1992, Chap. 10, pp. 391–452.

[14]Alcorn, C. W., Croom, M. A., and Francis, M. S., "The X-31 Experiment: Aerodynamic Impediments to Post-Stall Agility," AIAA Paper 95-0362, Jan. 1995.

[15]Smith, L. H., "Aerodynamic Characteristics of an Axisymmetric Body Undergoing a Uniform Pitching Motion," Ph.D. Dissertation, Naval Postgraduate School, Monterey, CA, Dec. 1974.

[16]Smith, L. H., and Nunn, R. H., "Aerodynamic Characteristics of an Axisymmetric Body Undergoing a Uniform Pitching Motion," *Journal of Spacecraft and Rockets*, Vol. 13, No. 1, 1976, pp. 8–14.

[17]Coe, P. L., Chambers, J. R., and Letko, W., "Asymmetric Lateral-Directional Characteristics of Pointed Bodies of Revolution at High Angles of Attack," NASA TND-7095, Nov. 1972.

[18]Allen, H. J., and Perkins, E. W., "Characteristics of Flow over Inclined Bodies of Revolution," NACA RM-A50L07, March 1951.

[19]Sarpkaya, T., "Separated Flow About Lifting Bodies and Impulsive Flow About Cylinders," *AIAA Journal*, Vol. 4, No. 3, 1966, pp. 414–426.

[20]Kamiya, N., Suzuki, S., Nakamura, M., and Yoshinaga, T., "Some Practical Aspects of the Burst of Laminar Separation Bubbles," International Council of the Aeronautical Sciences, ICAS-80- 10.2, Sept. 1980.

[21]Ericsson, L. E., "Effect of Transition on Wind Tunnel Simulation of Vehicle Dynamics," *Progress of Aerospace Sciences*, Vol. 27, 1990, pp. 121–144.